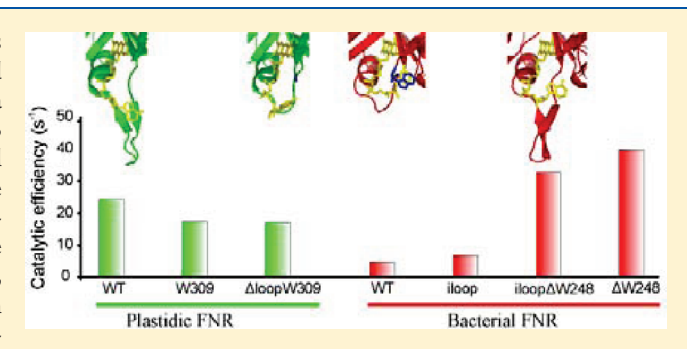


Swapping FAD Binding Motifs between Plastidic and Bacterial Ferredoxin-NADP(H) Reductases

Matías A. Musumeci, [†] Horacio Botti, [‡] Alejandro Buschiazzo, ^{‡,§} and Eduardo A. Ceccarelli*, [†]

Supporting Information

ABSTRACT: Plant-type ferredoxin-NADP(H) reductases (FNRs) are grouped in two classes, plastidic with an extended FAD conformation and high catalytic rates and bacterial with a folded flavin nucleotide and low turnover rates. The 112–123 β-hairpin from a plastidic FNR and the carboxy-terminal tryptophan of a bacterial FNR, suggested to be responsible for the FAD differential conformation, were mutually exchanged. The plastidic FNR lacking the β-hairpin was unable to fold properly. An extra tryptophan at the carboxy terminus, emulating the bacterial FNR, resulted in an enzyme with decreased affinity for FAD and reduced diaphorase and ferre-



doxin-dependent cytochrome c reductase activities. The insertion of the β -hairpin into the corresponding position of the bacterial FNR increased FAD affinity but did not affect its catalytic properties. The same insertion with simultaneous deletion of the carboxy-terminal tryptophan produced a bacterial chimera emulating the plastidic architecture with an increased $k_{\rm cat}$ and an increased catalytic efficiency for the diaphorase activity and a decrease in the enzyme's ability to react with its substrates ferredoxin and flavodoxin. Crystallographic structures of the chimeras showed no significant changes in their overall structure, although alterations in the FAD conformations were observed. Plastidic and bacterial FNRs thus reveal differential effects of key structural elements. While the 112-123 β -hairpin modulates the catalytic efficiency of plastidic FNR, it seems not to affect the bacterial FNR behavior, which instead can be improved by the loss of the C-terminal tryptophan. This report highlights the role of the FAD moiety conformation and the structural determinants involved in stabilizing it, ultimately modulating the functional output of FNRs.

The plant-type ferredoxin-NADP(H) reductases (FNRs) are ubiquitous enzymes that participate in a diverse array of metabolic processes, including photosynthesis, isoprenoid biosynthesis, oxidative stress response, xenobiotic detoxification, nitrogen and hydrogen fixation, steroid hydroxylation, and the synthesis of nucleotides and amino acids. $^{1-3}$

FNRs are typically composed of two domains, each of them containing approximately 150 amino acids.⁴ The carboxyl-terminal domain includes most of the residues involved in NADP(H) binding, while the prosthetic group FAD is mostly bound to the amino-terminal region at the interface between the two domains. The FAD isoalloxazine ring is stacked between two aromatic residues or an aromatic residue and an aliphatic residue.

FNRs can be further divided into two classes: a plastidic class characterized by an extended FAD conformation (Figure 1A,C) and high catalytic turnover rates for the diaphorase reaction using NADPH as a substrate $(100-600~{\rm s}^{-1})$ and a second class of bacterial proteins displaying a folded, bent conformation of FAD (Figure 1B,D) and very low turnover rates for the same reaction $(2-38~{\rm s}^{-1})$. The extended FAD conformation in plastidic FNRs is primarily obtained by the interaction of the AMP moiety

of FAD with a strand—loop—strand β -hairpin motif of the protein that is partially absent in bacterial FNRs (Figure 1A,B). In the latter enzymes, adenosine is stabilized in a bent conformation over the flavin, and an intramolecular hydrogen bond is typically observed between N-1 of the isoalloxazine ring and N-6 on the adenine moiety. Moreover, a carboxy-terminal extension that varies among different bacterial enzymes further stabilizes FAD binding by stacking an aromatic side chain over the adenine (Figure 1D). The relationship between this conformation of FAD and the activity of these enzymes has not been elucidated. A correlation between an extended FAD conformation with high catalytic efficiency in FNR enzymes has been suggested. Page 19.

We postulated that the striking differences in catalytic efficiencies between plastidic and bacterial FNRs are due in part to the effects of two distinct structures: (1) the β -hairpin of residues 112–123 involved in FAD binding in the plastidic enzyme,

Received: November 4, 2010 Revised: February 8, 2011 Published: February 09, 2011

[†]Molecular Biology Division, Instituto de Biología Molecular y Celular de Rosario (IBR), CONICET, Facultad de Ciencias Bioquímicas y Farmacéuticas, Universidad Nacional de Rosario, Suipacha 531, S2002LRK Rosario, Argentina

[‡]Unit of Protein Crystallography, Institut Pasteur de Montevideo, Mataojo 2020, Montevideo 11400, Uruguay

⁵Department of Structural Biology and Chemistry, Institut Pasteur, 25 rue du Dr Roux, Paris 75015, France

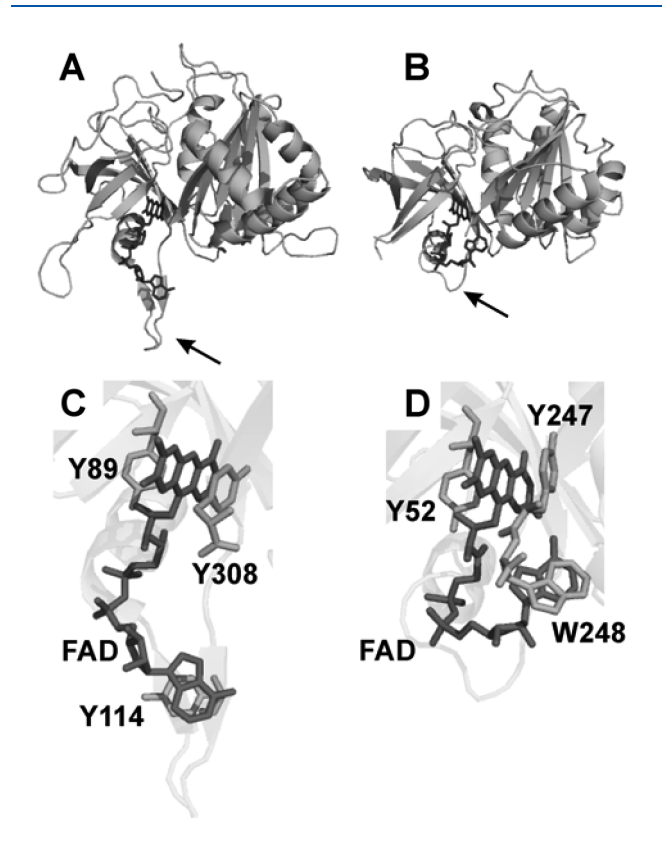


Figure 1. Prosthetic group binding in plastidic and bacterial FNRs. (A and B) Computer graphics based on X-ray diffraction data from (A) plastidic FNR (pea)²⁶ and (B) bacterial FNR (*Escherichia coli*).⁵ The arrows indicate the presence of the Val113—Lys123 β-hairpin in the plastidic enzyme and its absence in the bacterial one. (C and D) Details of the FAD (C) extended conformation as in plastidic FNR (as in pea FNR) and (D) bent conformation as in bacterial FNR (as in *E. coli* FNR). The aromatic residues interacting with the isoalloxazine and adenine portions of FAD are shown as light gray sticks.

which in the bacterial enzymes is replaced by a short amino acid stretch, and (2) the bulky lateral chain at the carboxyl terminus of the bacterial enzyme that is absent in the plastidic ones. To explain how the structural traits mentioned above may influence the function of these enzymes, we constructed the following working hypotheses. (1) In plastidic enzymes, the 112-123 β -hairpin element locates an aromatic residue for stacking with the FAD adenine in such a way that it stabilizes an extended prosthetic group conformation, optimizing the flavin arrangement and the accessibility of the substrate to the catalytic site. (2) The low turnover rates of the bacterial enzymes arise from (2a) the folded conformation of FAD, stabilized by the interaction of the prosthetic group with the hydrophobic carboxyl-terminal residue that affects the rate of access of the NADP(H) nicotinamide to the reaction site, and (2b) the establishment of a hydrogen bond between N6 of the adenine ring and N1 of the isoalloxazine, also facilitated by the bent conformation of the flavin.

To test these hypotheses, we constructed six chimeric plastidic and bacterial FNRs and characterized five of them. They were produced by exchanging the plastidic strand—loop—strand hairpin (amino acids 112—123), the short bacterial Val-Pro-Asp sequence, and the bacterial carboxy-terminal tryptophan residue, structures that are involved in FAD binding. The enzymes from pea and *Escherichia coli* were chosen as prototypes of plastidic and

bacterial FNRs, respectively. Given that *E. coli* FNR is a subclass II FNR, only this subgroup of bacterial enzymes is being considered here.

Overall, the results highlight the important roles of the strand—loop—strand cluster between amino acids 112 and 123 in the identification of more stable enzymes with higher FAD affinity. The presence of the β -hairpin and the absence of a bulky lateral chain at the C-terminus contribute to the high turnover rates observed for plastidic FNRs. Our observations are discussed with respect to the possible meanings of these findings with respect to the FNR enzyme catalytic efficiency.

EXPERIMENTAL PROCEDURES

Plasmid Construction. Wild-type and mutant pea and *E. coli* FNRs were overexpressed in *E. coli* as reported previously using vector pET205. This vector expresses a His-tagged thioredoxin—FNR fusion protein that contains a thrombin recognition site between the tag and the mature FNR. The construction of the different plastidic FNR and bacterial FNR variants and the sequences of the oligonucleotides used for cloning and mutagenesis are described in the Supporting Information. All cloned genes and constructs were confirmed by DNA sequencing.

Protein Expression and Purification. Flavodoxin, wild-type plastidic and bacterial FNRs, plastidic FNRW309, bacterial FNRiloop, bacterial FNR Δ W248, and bacterial FNRiloop Δ W248 were expressed in BL21DE3(plysS) E. coli cells induced with 0.25 mM IPTG at 25 °C for 6 h. Plastidic FNR∆loopW309 was expressed in E. coli cells induced with 0.10 mM IPTG at 15 °C for 16 h. After induction, cells were collected and recombinant enzymes were purified from the cell extracts by affinity chromatography using nickel-nitrilotriacetic acid agarose (QIAGEN, Valencia, CA) essentially as described previously. E. coli ferredoxin was expressed in *E. coli* cells as described for plastidic FNR∆loopW309 with the exception that the E. coli iron—sulfur gene cluster was coexpressed to improve yields. 10 Recombinant pea Fd was expressed in E. coli using vector pET28-Fd.8 Fd purification was performed as previously described.¹¹ The purity of all protein preparations was confirmed by sodium dodecyl sulfate-polyacrylamide gel electrophoresis (SDS-PAGE),¹² and protein concentrations were determined by UV-visible spectrophotometry.

Spectral Analyses. Absorption spectra were recorded on a Shimadzu UV-2450 spectrophotometer. CD spectra were obtained using a JASCO J-810 spectropolarimeter at 25 °C. The spectra were recorded in solutions having protein concentrations of 5.0 μ M for the near-UV and visible regions (250–600 nm) and 0.5 μ M for the far-UV region (200–250 nm) using 0.1 cm path length cuvettes. Fluorescence spectra were monitored using a Varian (Palo Alto, CA) Cary Eclipse fluorescence spectrophotometer interfaced with a personal computer. Samples were filtered through G25 Sephadex spin columns equilibrated with 50 mM potassium phosphate (pH 8.0) before measurements were taken. Extinction coefficients of the different plastidic FNR forms were determined by releasing FAD from the protein by treatment with 0.2% (w/v) SDS and quantifying the flavin spectrophotometrically. ¹³

Determination of Dissociation Constants of the Different Enzyme Variants in Complex with Nucleotides and Protein Substrates. The K_d values of the complexes between different plastidic and bacterial FNR variants and NADP⁺ were determined by difference absorption spectroscopy essentially as described previously. ¹⁴ Briefly, 15 μ M flavoprotein in 50 mM

Tris-HCl (pH 8.0) was titrated at 25 °C with NADP⁺. After each addition, the absorbance spectrum (200-600 nm) was monitored. Then, the difference spectra were calculated, and the absorbance differences at the stated wavelength were plotted versus the NADP+ concentration. The data were fitted to a theoretical equation for a 1:1 complex. In all cases, samples had been previously filtered through a desalting column equilibrated with 50 mM Tris-HCl (pH 8.0). To determine the K_d values of the complexes between different bacterial FNR variants and Fd, Fdx, or FldA, solutions containing 3 μ M enzyme in 50 mM Tris-HCl (pH 8.0) were titrated with the corresponding protein substrate. After each addition, the fluorescence quenching at 340 nm (excitation at 270 nm) was registered. Controls were run in parallel to estimate the fluorescence contribution due to the addition of Fd, Fdx, or Fld. The K_d values were estimated by fitting the fluorescence data to a theoretical equation for a 1:1 complex.

Thermal Unfolding Transitions. Protein stock solutions were diluted to a final concentration of 0.5 μ M in 50 mM potassium phosphate (pH 8.0). The CD signal was registered by excitation at 220 nm, while the temperature of the sample was increased at a uniform rate of 1 °C/min (from 15 to 80 °C). Thermal unfolding transitions were analyzed assuming a two-state approximation in which only the native and unfolded states are significantly populated. $T_{\rm M}$ was determined by fitting experimental data to the equation $\Delta G_{(T)} = \Delta H_{(T_{\rm M})} + \Delta C_p (T - T_{\rm M}) - T[\Delta H_{(T_{\rm M})}/T_{\rm M} + \Delta C_p \ln(T/T_{\rm M})]$, as described previously. Is

Enzymatic Assays. FNR-dependent NADPH-diaphorase and ferredoxin-dependent cytochrome c reductase activities were determined using published methods. 16 NADH-ferricyanide diaphorase activity was determined in a reaction medium (1 mL) containing 50 mM Tris-HCl (pH 8.0), 1 mM potassium ferricyanide, and 1.25–2.5 μ M FNR. The cytochrome c reductase activity of FNR, using either Fd, Fdx, or Fld, was assayed in a reaction medium (1 mL) containing 50 mM Tris-HCl (pH 8.0), 0.3 mM NADP⁺, 3 mM glucose 6-phosphate, 1 unit of glucose-6phosphate dehydrogenase, and 50 μ M cytochrome c. The cytochrome c reductase activity of bacterial FNR in the absence of protein mediators (e.g., ferredoxin or flavodoxin) was determined in a reaction medium (1 mL) containing 50 mM Tris-HCl (pH 8.0), 0.12 mM NADPH, and 100 μM cytochrome c. After the addition of approximately 15-100 nM FNR, cytochrome c reduction was monitored spectrophotometrically by following absorbance changes at 550 nm ($\varepsilon_{550} = 19 \text{ mM}^{-1} \text{ cm}^{-1}$). All kinetic experiments were performed at 30 °C. In all cases, precautions were taken to ensure the linearity of the enzyme activity determinations, and when appropriate, saturation of the Michaelis-Menten plots was verified.

Determination of the Dissociation Constants of the ApoFNR–FAD Complexes. Preparation of the apoprotein from pea and *E. coli* ferredoxin-NADP $^+$ reductases and the determination of $K_{\rm d}$ values for the dissociation of FNRs variants were performed using published methods. ¹⁷

Determination of FAD Dissociation Rate Constants ($k_{\rm off}$). The prosthetic group dissociation rate constant ($k_{\rm off}$) was determined by measuring continuously for 5 h the increase in the FAD fluorescence emission at 520 nm ($\lambda_{\rm exc}$ = 450 nm) of 5 μ M enzyme samples in 1 cm path lengths cells at 25 °C. Then the protein samples were denaturated with 0.2% (v/w) SDS, and the measured fluorescence arising from 100% free FAD was considered. The $k_{\rm off}$ values were calculated as the number of micromoles of FAD liberated per micromole of enzyme per

hour, assuming a 1:1 stoichiometry of the apoFNR—FAD complex. The initial fluorescence originated by the protein (time zero, 0% of free FAD) was subtracted from each measurement. Before the experiment, samples were filtered through a Sephadex G-10 (Sigma, St. Louis, MO) column equilibrated with 50 mM Tris-HCl (pH 8.0) to separate the free FAD.

Determination of Parameters. All experimental data were fitted to theoretical curves using Sigmaplot (Systat Software Inc., Point Richmond, CA).

Determination of the NADP⁺ Content of Bacterial FNRiloop∆W248 and Wild-Type Bacterial FNR Enzymes by HPLC Analysis. The enzyme preparation (final concentration of 25 μ M) was incubated with 6 M urea in ice for 1 h to release the bound NADP+, which was verified spectrophotometrically. Then, the NADP⁺ content was determined by HPLC analysis in an ÄKTA apparatus equipped with a UV absorption monitor (UV-900) and Unicorn 4.10 chromatography software (Amersham Biosciences). Samples were applied to a reverse phase C18 column (40 mm × 300 mm, Bio-Rad) equilibrated in 0.2 M KH_2PO_4 (pH 5.95). The column was then developed at a rate of 1 mL/min using a linear gradient of 80% (v/v) methanol in 0.2 M KH₂PO₄ (pH 5.95). The eluate was monitored at 260 and 450 nm. The NADP⁺ concentration was determined using an extinction coefficient of $17.8 \text{ mM}^{-1} \text{ cm}^{-1}$ at 260 nm. The FAD concentration was determined using an extinction coefficient of 11.3 mM⁻¹ cm⁻¹ at 450 nm and used as an internal control assuming a 1:1 protein:FAD stoichiometry.

Protein Crystallization and Data Collection. Crystals of plastidic FNR Δ loopW309 and bacterial FNRiloop Δ W248 were grown at 20 °C by the vapor diffusion method using a hanging drop setup. In the case of the plastidic FNR variant, droplets were set by mixing $2 \mu L$ of protein [4.5 mg/mL, stored in 50 mM Tris-HCl (pH 8.0)] with 2 μ L of reservoir solution containing 2.15 M ammonium sulfate (pH 8.0) and 100 mM Tris-HCl (pH 8.0). The droplet was equilibrated versus 1 mL of reservoir solution in sealed chambers. Microseeding was needed to obtain diffractionquality crystals. Orthorhombic crystals grew within 1-3 days. Cryoprotection was performed with progressive soaks (5 min each) via addition of 0.5 μ L aliquots of cryoprotectant solution [0.1 M Tris-HCl (pH 8.0), 2.9 M ammonium sulfate, and 30% (v/v) glycerol] to the crystal-containing droplets. This process was repeated eight times. Before being flash-frozen in liquid nitrogen, the crystals were rapidly soaked in a pure cryoprotectant solution. Crystals of bacterial FNRiloop∆W248 were grown following a similar approach. Two microliters of protein [10 mg/ mL in 50 mM Tris-HCl (pH 7.6)] was mixed with 2 μ L of a reservoir solution containing 0.2 M zinc acetate, 9% (v/v) PEG 8000, and 100 mM sodium cacodylate (pH 6.5). The droplet was equilibrated versus 1 mL of reservoir solution. Monoclinic crystals grew within 1-2 days. Crystals were cryoprotected via a quick soak in mother liquor containing 30% (v/v) glycerol. Single-crystal X-ray diffraction data sets were collected at 108 K using a Micromax007-HF (Rigaku) X-ray generator and a Mar345 (Mar Research) image plate detector following a standard single-angle oscillation strategy. Data collection statistics are summarized in Table 1.

Determination, Refinement, and Representation of Structure. The structures of both mutant proteins were determined by molecular replacement using AMoRe. The initial models employed in each case as search probes were the wild-type FNR structures from *Pisum sativum* (PDB entry 1QG0) and *E. coli* (PDB entry 1FDR). Small modifications were introduced

Table 1. X ray Diffraction Data Collection and Refinement Statistics

	plastidic FNR∆loopW309	bacterial FNRiloop Δ W248
space group	P2 ₁ 2 ₁ 2	C_2
wavelength (Å)	1.5418	1.5418
cell parameters	a = 113.4 Å, b = 140.2 Å, c = 51.2 Å	$a = 186.9 \text{ Å}, b = 74.6 \text{ Å}, c = 44.4 \text{ Å}, \beta = 101.8^{\circ}$
resolution (Å)	$28.9 - 2.9 (3.06 - 2.9)^a$	$28.9 - 1.9 (2 - 1.9)^a$
no. of unique measured reflections	18774	45215
multiplicity	4.6 (4.6) ^a	$3.8 (3.6)^a$
completeness (%)	99.7 $(100)^a$	95.8 (92.1) ^a
$R_{\text{meas}} (\%)^b$	$10(59.4)^a$	8.6 (48.8) ^a
$\langle I/\sigma(I) \rangle$	$11.7 (2.9)^a$	$12.8 (3.2)^a$
	Refinement	
resolution (Å)	28.04-2.9	27.8-1.9
R_{cryst} (%) ^c (no. of reflections)	19.6 (17796)	18.8 (44289)
R_{free} (%) ^c (no. of reflections)	23.4 (927)	22.3 (921)
rmsd for bond lengths (Å)	0.01	0.01
rmsd for bond angles (deg)	1.12	1.11
no. of protein non-hydrogen atoms	4571	3955
no. of water atoms	23	410
no. of ligand atoms	106 (2 \times FAD)/20 (4 \times sulfate)	96 (2 × NADP $^+$)/106 (2 × FAD)/12 (Zn $^{2+}$)/1
		$(3 \times \text{glycerol})/16 (2 \times \text{Tris})/1 (\text{Na}^+)$
PDB entry	2XNC	2XNJ

[&]quot;Values in parentheses apply to the highest-resolution shell. ${}^bR_{\rm meas} = \Sigma_h [N_h/(N_h-1)]^{1/2} \Sigma_i |I_i - \langle I\pm \rangle|/\Sigma_h \Sigma_i I\pm \rangle$, where N_h is the multiplicity for each reflection, I_i is the intensity of the ith observation of reflection h, $\langle I \rangle$ is the mean of intensity of all observations of reflection h, and $I\pm 1/N_h \Sigma_i [I_{(-)}]$ or $I_{(+)}$]. Σ_h is taken over all reflections, and Σ_i is taken over all observations of each reflection. ${}^cR = \Sigma_h |F(h)_{\rm obs} - F(h)_{\rm calc}|/\Sigma_h |F(h)_{\rm obs}|$. $R_{\rm cryst}$ and $R_{\rm free}$ were calculated using the working and test hkl reflection sets, respectively.

into the search model PDB structures before launching molecular replacement calculations, specifically removing the residues predicted to be affected by the protein engineering procedures, both on the β -hairpin loop and on the last carboxy-terminal Trp. In both structures, there were two monomers per asymmetric unit. Rotation and translation functions readily produced wellpacked solutions. Refinement was then performed using both REFMAC¹⁹ and BUSTER,²⁰ including the automatic identification of local noncrystallographic symmetry restraints (using BUSTER). TLS parameters were refined throughout and defined through two rigid bodies per monomer (residues 4-106 and 107-256 in E. coli bacterial FNR; residues 14-138 and 139-300 for the plastidic FNR from pea). The structure corresponding to the pea mutant enzyme showed density for the adenine ring of FAD chain C, sitting at <0.5 Å of the 2-fold axis. This was handled as a form of crystal disorder; all the atoms of the adenine heterocycle were thereafter refined at an occupancy of 0.5, and van der Waals nonbonded restraints were turned off (using Gelly EXCLUDE cards in BUSTER) to avoid symmetry-related repulsion. Figures were generated using PyMol (http://pymol.sourceforge.net/).

Entry Numbers. Atomic coordinates and structure factors have been deposited in the Protein Data Bank as entries 2XNC (plastidic FNR Δ loopW309) and 2XNJ (bacterial FNRiloop Δ W248).

RESULTS

Design and Construction of FNR Variants. The superimposed models corresponding to *E. coli* FPR (PDB entry 1FDR) and pea FNR (PDB entry 1QG0) and the details of the chimeric enzyme constructs are shown in Figure 2. Recombinant proteins

thereof were overexpressed, and five of them were purified and further characterized. The plastidic FNR chimera designated as plastidic FNR Δ loop was obtained via replacement of amino acids between positions 112 to 123 with the bacterial Val-Pro-Asp sequence. Another FNR chimera denoted plastidic FNRW309 contained an extra tryptophan at the carboxy terminus related to FAD binding in bacterial reductases. A third chimera denoted plastidic FNR Δ loopW309 was a combination of the other two chimeras, containing a deletion of the amino acid cluster and the carboxy-terminal tryptophan insertion (Figure 2B).

The chimera bacterial FNRiloop was constructed via replacement of the wild-type Pro71-Asp72 sequence with the corresponding plastidic FNR peptide sequence (including amino acids Val113—Lys123) (Figure 2B). The chimera bacterial FNR Δ W248 was obtained via deletion of the carboxy-terminal tryptophan, and a third chimera (bacterial FNRiloop Δ W248) was generated by simultaneously combining the two engineering procedures just described (Figure 2B).

The expression of the plastidic FNR variants in *E. coli* was analyzed using SDS-PAGE and Western blotting (Figure 2C). The plastidic FNRΔloop enzyme was always found to form insoluble aggregates despite a number of different bacterial overexpression conditions being tested. No further analysis was thus possible with this particular construct. Interestingly, the incorporation of a tryptophan as the carboxy-terminal residue (chimera plastidic FNRΔloopW309) partially restored the folding during protein expression (Figure 2C). Accordingly, with the exception of plastidic FNRΔloop, all flavoenzyme variants were expressed as soluble proteins, purified, and obtained as homogeneous preparations as judged by SDS-PAGE (not shown).

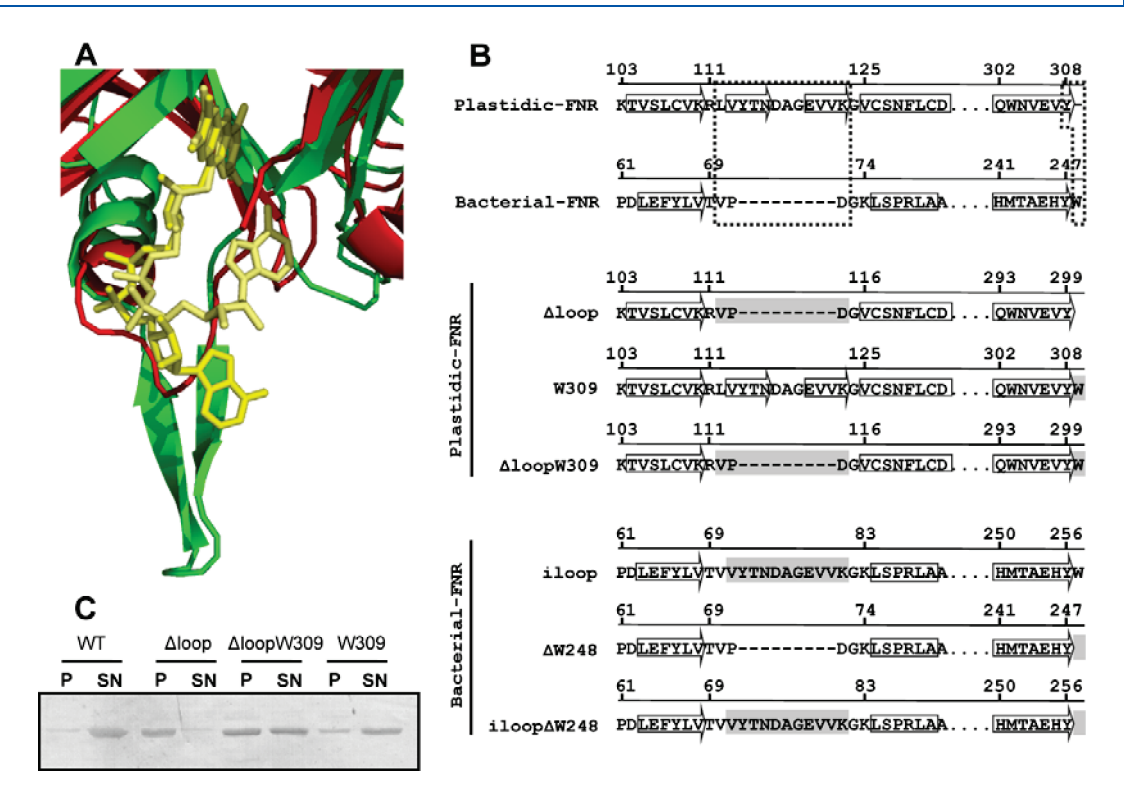


Figure 2. Construction of the different plastidic and bacterial FNR variants. (A) Superposition of the crystal structures of the plastidic FNR from pea (green; FAD colored yellow) and the bacterial FNR form *E. coli* (red; FAD colored light yellow). Only relevant regions are shown. (B) Sequences of the wild-type and mutant plastidic and bacterial FNRs. The dotted boxes show the regions that were modified. Arrows and boxes represent β-strand and α-helix structural elements, respectively. Introduced mutations are shown in gray boxes. (C) Western blot analysis of plastidic FNR mutants after their overexpression in *E. coli*. P denotes a pellet or insoluble fraction. SN denotes a supernatant or soluble fraction.

Spectral Properties. Analysis of the UV—visible absorption properties of the different plastidic FNR variants showed small changes in intensities but not in maxima, suggesting only slight variations in the FAD isoalloxazine environment (Figure 3A). In contrast, both bacterial FNR Δ W248 and bacterial FNRiloop Δ W248 mutants exhibited spectral differences with respect to the corresponding wild-type bacterial FNR. To facilitate the comparison of data, the wild-type plastidic FNR spectrum is included in Figure 3B. The spectra of the bacterial mutants displayed a shift in the transition band maximum from 400 to 383 nm that was accompanied by a decrease in the intensity of the peak, resulting in spectra similar to those found for the wild-type plastidic FNR.

Structural Integrity and Conformation. In all cases, near-UV and visible CD spectra of the plastidic FNR variants were very similar in shape to that obtained for the wild-type plastidic FNR (Figure 3C). In contrast, differences were observed in the near-UV and visible CD spectra for the bacterial FNR chimeras with respect to the wild-type bacterial enzyme (Figure 3D). An intensity decrease at 274 nm was observed along with a blue shift to 270 nm. Simultaneously, a new minimum appears at 285 nm in bacterial FNR Δ W248 and bacterial FNRiloop Δ W248 flavoenzymes. Additionally, in these mutants, the typical peak at 389 nm found in the *E. coli* wild-type bacterial FNR was shifted to 378 nm.

Thermal Analysis of Protein Unfolding and FAD Affinity. Table 2 shows the unfolding transition melting point $(T_{\rm M})$ for the mutant proteins being analyzed. The replacement of the β -hairpin comprising Leu112—Lys123 in the plastidic enzyme with a Val-Pro-Asp sequence was detrimental for the stability of the enzyme. Consistently, the insertion of this structure into the

bacterial enzyme produced a more stable protein. In contrast, the deletion of Trp248 destabilized the recombinant protein [bacterial FNR Δ W248 (Table 2)]. This destabilization can be partially reversed by the introduction of the loop sequence from the pea enzyme (Val113—Lys123) as observed for bacterial FNRiloop Δ W248.

In line with the decrease in thermal stability associated with the replacement of the Leu112—Lys123 loop region with the Val-Pro-Asp sequence, FNR Δ loopW309 displayed a FAD affinity 1 order of magnitude lower than that of wild-type plastidic FNR, whereas the affinity of the variant plastidic FNRW309 for the flavin moiety did not change significantly (Table 2). Bacterial FNR Δ W248 $K_{\rm d}$ quantification could not be done, since the apoprotein precipitated during its preparation.

We have observed that the noncovalently bound FAD is slowly released into the medium by wild-type plastidic and bacterial FNRs. It is then feasible to measure the dissociation rate constant k_{off} for the prosthetic group. The rate of FAD dissociation was thus measured following FAD fluorescence because it is strongly quenched when bound to the enzyme. Table 2 shows an increase in k_{off} for FAD for plastidic FNR Δ loopW309 with respect to the wild-type enzyme. In agreement with these results, the wild-type bacterial FNR and bacterial FNR Δ W248 exhibited higher k_{off} values than the variant, including the inserted loop. Moreover, the incorporation of the Val113-Lys123 β -hairpin region into the bacterial enzyme (variants bacterial FNRiloop and bacterial FNRiloop Δ W248) generated more stable forms that were able to properly bind FAD in vitro. The FAD K_d values for these forms were similar to the affinity values observed with the plastidic FNR (Table 2).

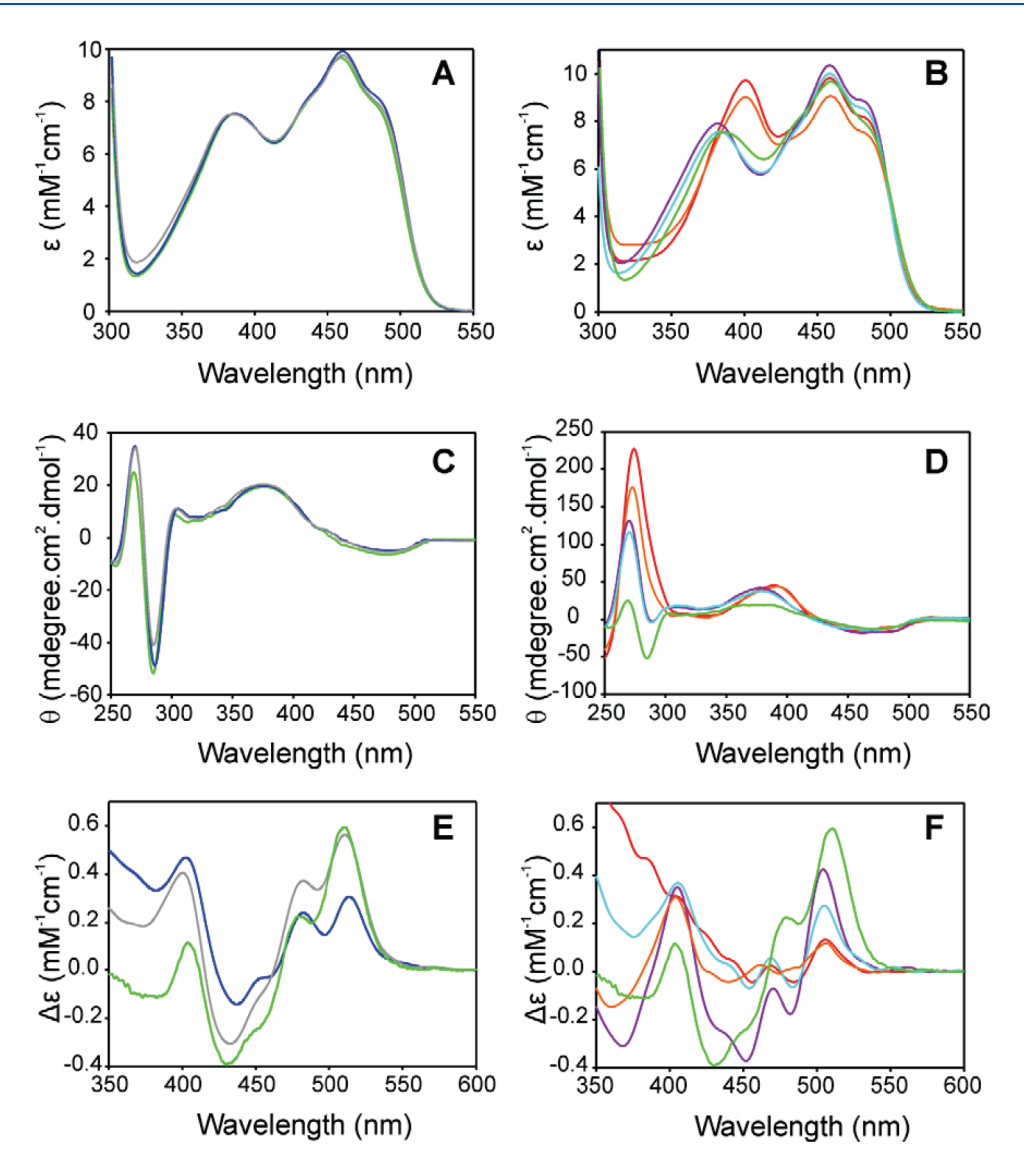


Figure 3. Spectroscopic analysis of the wild-type and mutant forms of the plastidic and bacterial FNRs. (A and B) UV—visible absorption spectra, (C and D) near-UV and visible CD spectra, and (E and F) difference absorption spectra elicited by the addition of NADP $^+$. For plastidic enzymes (A, C, and E), the following line colors were adopted: green for wild-type plastidic FNR, blue for plastidic FNR Δ loopW309, and gray for plastidic FNRW309. The bacterial enzymes (B, D, and F) were represented as follows: red for wild-type bacterial FNR, orange for bacterial FNRiloop, violet for bacterial FNR Δ W248, and cyan for bacterial FNRiloop Δ W248. The wild-type plastidic FNR spectra (green) were included in panels B, D, and F to facilitate analysis of data.

Interactions with Substrates and Steady-State Kinetics. The $K_{\rm d}$ values of the complexes of different plastidic and bacterial FNR variants with NADP⁺ were determined by difference absorption spectroscopy as described previously¹³ with minor modifications (Table 3). The spectral changes obtained by incubation of the wild-type and mutant enzymes with NADP⁺ are shown in panels E and F of Figure 3. NADP⁺ binding to the plastidic FNRW309 variant induced spectral changes similar in shape and intensity to that of the wild-type enzyme, with a recognized maximum at 510 nm that has been reported to correlate with the nicotinamide interaction on the re face of the isoalloxazine. ^{13,21,22} In contrast, mutant plastidic FNR Δ loopW309 exhibited a decrease in this maximum (Figure 3E). Nevertheless, these phenomena were accompanied by only small changes in the $K_{\rm d}$ (Table 3), with the plastidic FNRW309 variant exhibiting the larger value.

The spectral perturbations observed for bacterial FNRiloop, bacterial FNR Δ W248, and bacterial FNRiloop Δ W248 and the

wild-type enzyme upon NADP⁺ binding are shown in Figure 3F. Spectra of the variants from which the terminal tryptophan had been deleted were very different from those observed for the wild-type and iloop bacterial FNRs and similar in shape to those observed for the pea FNR mutant Y308S^{21,23} and the *Anabaena* FNR mutant Y303S,²⁴ which are both plastidic enzymes. The most remarkable feature is an increase in the intensity of the peak at 510 nm, suggesting a greater occupancy of the nicotinamide binding site in bacterial FNR Δ W248 and bacterial FNRiloop Δ W248 variants. The NADP⁺ dissociation constants were not significantly affected in any of the bacterial mutants (Table 3), indicating that amino acids and structures related to nucleotide binding remained unaltered.

The catalytic properties of the different plastidic and bacterial FNR variants were determined for three different enzymatic reactions. The observed $k_{\rm cat}$ and $K_{\rm M}$ values and the calculated $k_{\rm cat}/K_{\rm M}$ values for the NADPH-diaphorase reaction were

Table 2. Estimation of Protein Stability Derived from the Thermally Induced Unfolding Curves and FAD Affinity of Wild-Type and Mutant Forms of Plastidic and Bacterial FNRs

	enzyme	T_{M}^{a} (°C)	$\Delta T_{ m M}^{b}$ (°C)	$K_d(FAD)^c(nM)$	$k_{\text{off}}^{}} \left[\mu \text{mol of FAD h}^{-1} \left(\mu \text{mol of FNR} \right)^{-1} \right]$
plastidic FNR	wild-type	61.5 ± 0.5		6.3 ± 0.2	$1.1 \times 10^{-5} \pm 1 \times 10^{-6}$
	W309	59.5 ± 1.2	-2.0 ± 0.7	8.1 ± 0.2	$3.7 \times 10^{-5} \pm 2 \times 10^{-6}$
	Δ loopW309	56.4 ± 0.9	-5.1 ± 0.4	64.2 ± 0.3	$1.8 \times 10^{-3} \pm 1 \times 10^{-4}$
bacterial FNR	wild-type	57.5 ± 0.7		not determined	$1.6 \times 10^{-2} \pm 4 \times 10^{-4}$
	iloop	58.7 ± 0.6	1.2 ± 0.1	1.2 ± 0.7	$1.7 \times 10^{-3} \pm 7 \times 10^{-5}$
	Δ W248	51.7 ± 0.3	-5.8 ± 0.4	not determined	$6.5 \times 10^{-2} \pm 6 \times 10^{-4}$
	iloop Δ W248	53.4 ± 0.8	-4.1 ± 0.1	1.1 ± 0.09	$3.4\times10^{-2}\pm1\times10^{-4}$

^a $T_{\rm M}$ is the temperature of the midpoint of the thermal denaturation transition. ^b $\Delta T_{\rm M}$ is the difference between the $T_{\rm M}$ of the mutant protein and that of the corresponding wild-type enzyme, estimated as described in Experimental Procedures. ^c Determined as described in Experimental Procedures.

Table 3. Kinetic Parameters^a of the NADPH- and NADH-Diaphorase Reactions Catalyzed by Wild-Type and Mutant Forms^b and Dissociation Constants for the Different Complexes with NADP⁺ of Plastidic and Bacterial FNRs

		NADPH				NADH			
		k_{cat} (s ⁻¹)	$K_{ m M}$ $(\mu{ m M})$	$\frac{k_{\rm cat}/K_{\rm M}}{({\rm s}^{-1}\mu{\rm M}^{-1})}$	$K_{ m d}({ m NADP}^+) \ (\mu{ m M})$	k_{cat} (s^{-1})	$K_{ m M}$ (mM)	$\frac{k_{\rm cat}/K_{\rm M}}{({\rm s}^{-1}\mu{\rm M}^{-1})}$	NADPH/NADH specificity ^c
plastidic FNR	wild-type	374.3 ± 18	15.3 ± 4.3	24.5	10.9 ± 3.1	7.0 ± 2.1	14.3 ± 3.9	5×10^{-4}	49000
	W309	360.5 ± 12	20.7 ± 3.9	$17.4 (71\%)^d$	22.1 ± 3.2	5.0 ± 1.2	5.9 ± 1.2	8×10^{-4}	21750
	Δ loopW309	251.1 ± 14	14.7 ± 2.0	17.1 (70%)	18.6 ± 1.3	2.0 ± 0.3	3.7 ± 0.9	6×10^{-4}	28433
bacterial FNR	wild-type	38.2 ± 3.5	8.3 ± 1.3	4.6	5.9 ± 0.6	<0.05 ^e	Nd^f	Nd^f	_
	iloop	24.5 ± 2.0	3.6 ± 0.8	6.8 (148%)	6.3 ± 0.4	<0.05 ^e	Nd^f	Nd^f	_
	Δ W248	95.5 ± 4.8	2.4 ± 0.7	39.8 (865%)	5.7 ± 0.5	54.1 ± 5.6	$\textbf{6.5} \pm \textbf{0.6}$	8×10^{-3}	4975
	iloop Δ W248	99.0 ± 3.5	3.0 ± 0.7	33.0 (717%)	7.5 ± 0.8	45.3 ± 3.5	3.0 ± 0.8	1.5×10^{-2}	2062

^a Each parameter value represents the average of three independent. Description of the calculation method employed is reported in Experimental Procedures. ^b Potassium ferricyanide reduction was assessed using the diaphorase assay of Zanetti¹⁶ in 50 mM Tris-HCl (pH 8.0) using NADPH or NADH as the substrate. ^c Estimated as $(k_{cat}/K_M)^{NADPH}/(k_{cat}/K_M)^{NADH}$. ^d Values in parentheses represent the percentages of the observed value for each variant with respect to that of the wild-type enzyme. ^c An estimate of the limit of the determination based on the tested sensitivity of the method. ^f Not determined.

obtained at a fixed saturating concentration (1 mM) of potassium ferricyanide (Table 3). Plastidic FNRW309 and plastidic FNR Δ loopW309 exhibited k_{cat}/K_{M} values \sim 0.7-fold lower than those observed for the wild-type enzyme. The wild-type bacterial FNR and the bacterial FNRiloop variant exhibited similar k_{cat} K_M values for the NADPH-diaphorase reaction. In contrast, bacterial FNR∆W248 and bacterial FNRiloop∆W248 variants exhibited $k_{\rm cat}/K_{\rm M}$ values almost 9-fold higher than that of wildtype bacterial FNR, resulting from a 3-fold increase in the k_{cat} values and a decrease in the $K_{\rm M}$ values. Thus, the observed $k_{\rm cat}/$ K_M values for these variants were even higher than the one observed for the plastidic FNR. The bacterial enzyme has the ability to reduce cytochrome c in the absence of flavodoxin or other alternative protein mediators (e.g., ferredoxin).²⁵ Using saturating concentrations of cytochrome c, we observed activity increases of 239 and 210% for bacterial FNR Δ W248 (5.06 \pm $0.31~{\rm s}^{-1}$) and bacterial FNRiloop Δ W248 ($4.46\pm0.22~{\rm s}^{-1}$) with respect to that of the wild-type bacterial FNR $(2.12 \pm 0.12 \text{ s}^{-1})$, respectively.

The kinetic parameters of the different plastidic and bacterial FNR variants with pea and $E.\ coli$ ferredoxins (which contain a [2Fe-2S] cluster) and $E.\ coli$ flavodoxin A (containing a non-covalently bound FMN cofactor) are listed in Table 4. Plastidic FNR Δ loopW309 and plastidic FNRW309 variants exhibited a 53–57% reduction in $k_{\rm cat}$ relative to that of the wild-type enzyme. Given that the $K_{\rm M}$ for pea ferredoxin has decreased by the same extent, the apparent catalytic efficiency remained

unchanged. The bacterial FNR∆W248 and bacterial FNRiloopΔW248 variants exhibited a notable decrease in catalytic activity when ferredoxin from pea (Fd) and ferredoxin from E. coli (Fdx) were used as substrates and an extremely low activity with flavodoxin, one of the physiological substrates of the wildtype enzyme, precluding the possibility of properly measuring kinetic parameters. Likewise, the deletion of the carboxy-terminal tryptophan produced enzymes that were 3.3- and 8.3-fold less efficient with Fdx than the wild-type bacterial enzyme. Thus, although the bacterial FNR mutants lacking the carboxy-terminal tryptophan exhibited increased catalytic efficiencies with small electron acceptors, we observed a significant decrease in enzyme activity with the physiological protein electron carriers. To further analyze this issue, we determined the affinity of the wild-type and mutant bacterial FNR variants in complex with pea ferredoxin or bacterial flavodoxin. We determined that neither the introduction of the β -hairpin nor the deletion of the carboxy-terminal tryptophan affected significantly the binding of pea ferredoxin, E. coli flavodoxin A, or E. coli ferredoxin to the bacterial FNR (Table S2 of the Supporting Information).

To investigate whether the ability of the mutants to interact with the NADP(H) nicotinamide was modified, we analyzed the ability of the different plastidic and bacterial FNR forms to discriminate between NAD(H) and NADP(H) as substrates. Although the plastidic FNR variants exhibited decreases in both $K_{\rm M}$ and $k_{\rm cat}$ values for NADPH, they ultimately display a 50% reduction in their capacities to discriminate NADPH from

Table 4. Kinetic Parameters^a for Cytochrome c Reductase of the Wild-Type and Mutant Forms of Plastidic and Bacterial FNRs with Pea Ferredoxin, E. coli Flavodoxin A, and E. coli Ferredoxin^b

		pea ferredoxin			E. coli flavodoxin A			E. coli ferredoxin		
		k_{cat} (s^{-1})	<i>K</i> _M (μM)	$k_{\text{cat}}/K_{\text{M}}$ $(s^{-1} \mu \text{M}^{-1})$	k_{cat} (s^{-1})	$K_{ m M}$ $(\mu{ m M})$	$k_{\text{cat}}/K_{\text{M}}$ $(s^{-1} \mu \text{M}^{-1})$	k_{cat} (s^{-1})	$K_{ m M}$ $(\mu{ m M})$	$k_{\rm cat}/K_{\rm M}$ $({\rm s}^{-1}\mu{\rm M}^{-1})$
plastidic FNR	wild-type	75.0 ± 0.5	2.2 ± 0.2	34.1	Nd^c	Nd^c	Nd^c	Nd^c	Nd^c	Nd^c
	W309	35.9 ± 0.2	0.9 ± 0.4	39.8	Nd^c	Nd^c	Nd^c	Nd^c	Nd^c	Nd^c
	Δ loopW309	32.7 ± 0.3	0.9 ± 0.3	36.3	Nd^c	Nd^c	Nd^c	Nd^c	Nd^c	Nd^c
bacterial FNR	wild-type	22.8 ± 0.2	1.4 ± 0.1	16.3	8.9 ± 1.0	2.3 ± 0.2	3.9 ± 0.2	12.3 ± 1.2	$\boldsymbol{0.074 \pm 0.023}$	164.9
	iloop	19.4 ± 0.2	1.8 ± 0.1	10.7	7.5 ± 0.9	2.6 ± 0.2	2.9 ± 0.4	12.8 ± 1.0	$\boldsymbol{0.095 \pm 0.018}$	133.82
	Δ W248	4.6 ± 0.1	6.2 ± 0.4	0.74	<0.1 ^d	Nd^c	Nd^c	1.4 ± 1.0	0.070 ± 0.033	19.9
	iloop Δ W248	3.7 ± 0.2	7.6 ± 0.3	0.50	<0.1 ^d	Nd^c	Nd^c	1.2 ± 0.5	0.024 ± 0.015	50.0

^a Each parameter value represents the average of three independent experiments. Description of the calculation method employed is reported in Experimental Procedures. ^b Cytochrome c reduction was followed at 550 nm ($\varepsilon_{550} = 19 \text{ mM}^{-1} \text{ cm}^{-1}$) as described in Experimental Procedures. ^c Not determined. ^d An estimate of the limit of the determination based on the tested sensitivity of the method.

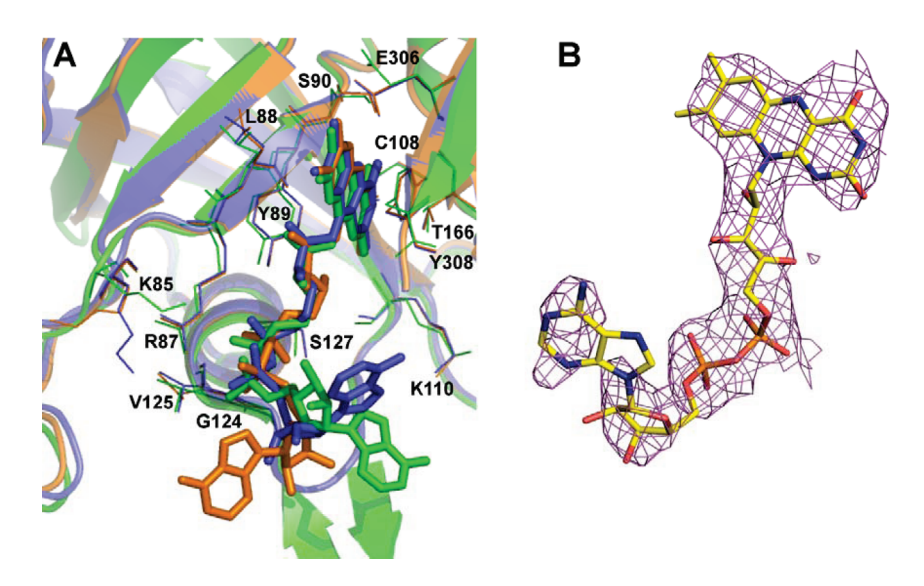


Figure 4. Crystal structure of plastidic FNR Δ loopW309 at 2.9 Å resolution. (A) Comparison of the FAD binding site between each monomer (blue and orange) and wild-type pea FNR (green) as a result of the overall structural alignment. The labeled residues correspond to the structure of the wild-type enzyme. (B) Close-up of the FAD molecule bound to monomer B (blue chain in panel A), showing a Fourier electron density map (sigma-A-weighted $2mF_{\rm obs} - DF_{\rm calc}$ map, contoured at 1σ). Note the absence of continuity, mainly involving the adenosine moiety toward the bottom of the figure.

NADH (Table 3). In contrast, the bacterial FNR Δ W248 and bacterial FNRiloop Δ W248 *E. coli* variants readily catalyzed the diaphorase reaction with NADH, while the wild-type bacterial enzyme exhibited extremely low enzymatic activity with NADH. The deletion of the carboxy-terminal tryptophan but not the insertion of the loop greatly enhanced the $k_{\rm cat}$ with NADH. The observed NADPH versus NADH specificities of these variants were 10- and 20-fold lower than those observed for the plastidic FNRs variants and the wild-type forms, respectively (Table 3).

Crystal Structures of the Plastidic FNR Δ loopW309 and Bacterial FNRiloop Δ W248 Variants. The three-dimensional structures of plastidic FNR Δ loopW309 and bacterial FNRiloop Δ W248 were determined by molecular replacement using single monomers of the wild-type pea plastidic FNR (PDB entry 1QG0) and *E. coli* bacterial FNR (1FDR), respectively, as search probes. The structures were then refined to 2.9 Å (plastidic FNR) and 1.9 Å (bacterial FNR) resolution with a maximum likelihood target function, as implemented in BUSTER (Table 1).

Compared to the wild-type enzyme, ²⁶ plastidic FNR∆loopW309 crystallized in a different crystal form, most probably because of the key role of the deleted loop in establishing wild-type crystal contacts. Plastidic FNR∆loopW309 shows two monomers in the asymmetric unit, both sharing a structure very similar to that of the wild-type enzyme (0.38 Å rmsd, superimposing 256 C α atoms). The inserted C-terminal tryptophan in plastidic FNR∆loopW309 was detected in both monomers, with clear difference Fourier peaks corresponding to W309 main chain atoms. However, no electron density signal above the noise level could be detected for their side chains (Figure S1 of the Supporting Information), strongly suggesting high mobility and ultimately not allowing the inclusion of W309 side chains in the final model. The FAD molecules are seen tightly bound to the enzyme, respecting a similar binding organization as in the wild-type form (Figure 4A), as well as in other plastidic FNRs. 26 In particular, no significant changes were observed between plastidic FNRΔloopW309 and the wild-type enzyme, with respect to the stacking arrangement between Tyr308 (Tyr299 in the plastidic FNR∆loopW309 numbering) and the isoalloxazine ring. FAD

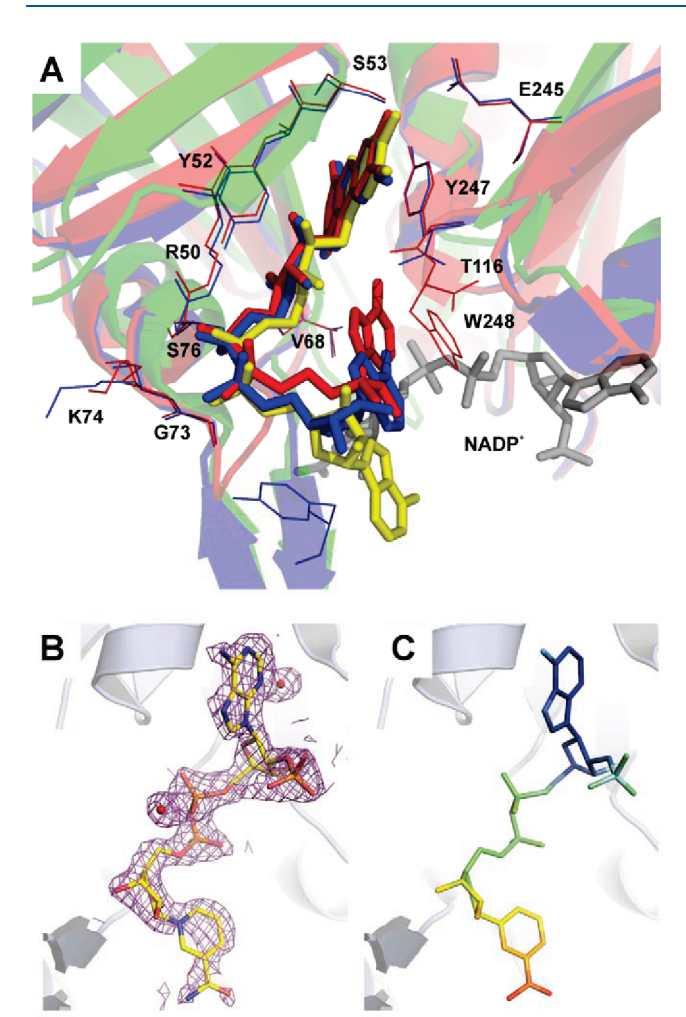


Figure 5. Crystal structure of bacterial FNRiloopΔW248 at 1.9 Å resolution. (A) View of the FAD binding sites after superimposition of mutant bacterial FNRiloopΔW248 (blue) with wild-type bacterial and plastidic FNRs (red and green; FAD colored yellow). (B) Electron density map $(2mF_{\rm obs}-DF_{\rm calc})$ contoured at 1σ) of only the NADP+bound to mutant bacterial FNRiloopΔW248 (for the sake of clarity). The nicotinamide ring is drawn toward the bottom of the figure. (C) NADP+ atoms colored according to their B factors [color ramp from blue (corresponding to low B factors), through green, to red (corresponding to the highest B factors)].

adopts similar conformations in both monomers, except for the adenine and ribose moieties of the AMP nucleotide portion, revealing low electron density values (Figure 4B) or even crystal disorder (Figure S2 of the Supporting Information), consistent with high mobility.

The bacterial FNRiloop Δ W248 variant crystallized with two monomers in the asymmetric unit, again revealing a different crystal packing compared to that of the wild-type enzyme. Both structures show a high degree of similarity, with a 0.45 Å rmsd over 235 aligned residues. Superposition of FNR structures using isoalloxazine to fit them shows a different final FAD adenine conformation between bacterial FNRiloop Δ W248 and the wild-type bacterial enzyme, with significant separation of N1 of the isoalloxazine ring from N6 of the adenine ring (Figure 5A). An unexpected outcome was the unambiguous identification of bound NADP in both monomers, revealing a conserved binding pattern when compared to previous reports. As opposed

to the 2'P-AMP portion of the dinucleotide, which is well fixed through extensive binding to the protein pocket, the nicotinamide rings are quite mobile in both monomers of the asymmetric unit, displaying low electron density and high B factors (Figure 5B,C). The best conformation has been modeled according to the Fourier maps, although weak difference Fourier features do not exclude the presence of alternative conformations, which appear to include closer interactions between the nicotinamide and the isoalloxazine rings. A few key residues are not conserved in plastidic FNRs, in particular E. coli residues Arg193 (replacing a Tyr), Asp229 (Gly), and Asn223 (Leu), all fixing the adenylate nucleotide of NADP⁺. The NADP⁺ contents of the purified wild type and different bacterial FNR variants used for crystallization studies were analyzed by reverse phase HPLC. In all cases, a nucleotide:enzyme molar ratio of 0.1 was found (not shown). Analysis of plastidic variants purified by the same procedure showed that neither the wild type nor the mutants contained bound NADP⁺.

DISCUSSION

The aim of this work was to investigate the role of the 112–123 β -hairpin of plastidic FNR and the carboxyl-terminal tryptophan of subclass II bacterial FNRs in FAD conformation, enzyme structure, and enzyme function. We postulate that the striking differences in catalytic efficiencies between plastidic and bacterial FNRs are due in part to the effects of these two distinct structures, which would be related to the FAD conformation.

To test these hypotheses, six chimeric plastidic and bacterial FNRs, containing different exchanged fragments involved in FAD binding, were constructed and five of them characterized.

Effects of the Deletion of the 112–123 β -Hairpin and the Insertion of a Tryptophan at the Carboxy Terminus of Plastidic FNR from Pea. The extended conformation of FAD locates the adenine ring far from the active site. It has thus been suggested that structural variations in that region of the protein should have a minor impact on catalysis. 4,29 The crystallographic structure of pea plastidic FNR∆loopW309 shows that the introduced mutations were not able to completely fold the FAD to a similar extent as observed in wild-type E. coli bacterial FNR. None of the remaining key amino acids involved in FAD binding were modified upon protein engineering, and actually, their conformations were not altered upon deletion of the 112-123 β -hairpin. Further comparison between the crystal structures of the proteins with and without the β -hairpin showed no significant changes in the position of the isoalloxazine or in the angle of the isoalloxazine with respect to the tyrosines that interact from both sides of the flavin (Figure S1 of the Supporting Information), at the level of precision of both models. Taking all of it into account, we can conclude that the concomitant deletion of the β -hairpin and the inclusion of the extra terminal tryptophan did not change significantly the overall structure of the plastidic enzyme. A decrease in the affinity of the apoprotein for the prosthetic group FAD and the overall protein stability as observed via a decrease in the T_{M} values suggest that the 112-123 β -hairpin is mainly involved in binding of the prosthetic group. However, we did observe alterations in the catalytic activities, with both surrogate (33% inhibition) and physiological (56% inhibition) substrates. Given that functional analyses of the plastidic FNR∆loop variant were not possible, the effect of the extra Trp at the C-terminus is not excluded.

The overall enzyme reaction may be limited if the NADP(H) nicotinamide is impaired from interacting productively with the isoalloxazine or if nucleotide exchange within and outside the catalytic site is affected. Steric hindrance for facile nicotinamide—isoalloxazine interaction could be relevant in overall catalytic efficiency modulation, even moreso considering that it has been determined that the FNR reductive half-reaction, the transfer of the hydride from NADPH to the FAD, is the rate-limiting step for the ferricyanide NADPH-diaphorase. There are several reports indicating that the nucleotide exchange rate should be optimized to allow the observed high catalytic rates in these enzymes. 9,14,24,30

The magnitude of the spectral changes upon binding of NADP⁺ to the enzyme at 510 nm can be taken as a comparative indication of the interaction between the isoalloxazine and the NADP(H) nicotinamide. A decrease in the magnitude of the peak at this wavelength was observed for the plastidic FNR Δ loopW309 variant. Tyr308, which is regarded as the key element in regulating the interaction of the nicotinamide with the isoalloxazine, was found at a similar position in the plastidic FNR Δ loopW309 variant and in the wild-type enzyme. Thus, some steric constraints between the folded conformations of FAD and/or the adenosine moiety (which display high mobility) with the NADP⁺ nicotinamide moiety could impair the catalytic process in the mutants. The bulky carboxy-terminal tryptophan can be a direct means for steric hindrance and reduction of catalysis.

Effects of the Deletion of the Carboxyl-Terminal Tryptophan and Insertion of the β -Hairpin on the NADPH-Diaphorase Activity of Bacterial FNR. The crystal structures of plastidic wild-type FNRs show that NADP+ binds to these enzymes in a nonproductive form where the nicotinamide is far from the isoalloxazine.^{27,31} These observations have been also obtained for bacterial FNRs (refs 6 and 32 and this work). It is proposed that NADP(H) binds to FNRs by a bipartite mechanism (refs 2, 23, 24, and 30 and this work). In the subclass I bacterial FNR from Rhodobacter capsulatus, the existence of charge-transfer complexes prior to hydride exchange was detected.²⁸ We can conclude that catalysis in bacterial and plastidic FNRs occurs with the stacking of the nicotinamide on the flavin. Consequently, it can be suggested that several conformational changes of the coenzyme should occur during catalysis for recognition and productive binding, which has been previously postulated for the E. coli FNR^{7,33} and for the bacterial FNR from Pseudomonas aeruginosa. 32 The bent conformation of FAD or the absence of a flexible region in the plastidic mutant may force the system to perform a larger molecular organization, thus decreasing the catalytic efficiency of the enzyme. This hypothesis is well supported by the data obtained with the bacterial variants. An increase in diaphorase activity was observed with a concomitant decrease in $K_{\rm M}$ for NADPH in bacterial FNR variants where the interaction of the carboxy-terminal tryptophan and the FAD adenine was abolished by mutation. Diaphorase reaction kinetic data indicated that in bacterial FNR, the transfer of electrons from NADPH to the flavin is the limiting step of the reaction.^{7,33} Moreover, from stopped-flow and steadystate kinetic studies, it has been determined that the reduction of cytochrome c in the absence of flavodoxin or ferredoxin by the E. coli bacterial FNR is rate-limited by processes other than its binding or the transfer of an electron to the ferric heme.²⁵ Thus, the observed increment on the cytochrome c reduction by the bacterial FNR variants lacking the carboxy terminus also supports the notion that the catalytic step involving FAD reduction

has been enhanced. Therefore, it may be concluded that this step was improved in our bacterial FNR mutants by avoiding the FAD bent conformation and/or by removing the obstruction that the carboxyl-terminal tryptophan imposes on the substrate entrance with consequent enhanced activity during NADP(H)-dependent catalysis.

The spectral changes observed in the bacterial FNR Δ W248 and bacterial FNRiloop Δ W248 variants indicate that the loss of the tryptophan allows for a greater amount binding in its presumed productive position. An increase in the degree of occupancy of the nicotinamide in the catalytic site could explain a higher rate of turnover for the enzyme with their natural nucleotide substrate as well as the observed higher rates with NADH seen for these mutants. An increased NADH-diaphorase activity was observed in plastidic enzymes in which the carboxy-terminal tyrosine was mutated to serine. 21,24,34 An increment in the interaction of the nicotinamide of NADH with the flavin was indicated as the cause for the increase in the activity with this nucleotide in plastidic FNRs. 21,24 In good agreement with these conclusions is the observation that adding a carboxyl-terminal tryptophan only partially affects the catalytic efficiency of the plastidic FNR, because this residue does not force the FAD to change its conformation completely, as shown in the obtained crystal data. Our results also showed that there are other sequence differences in these proteins that dictate whether the FAD is more stretched versus folded back and that this information is not simply coded in the β -hairpin and a carboxy-terminal tryptophan.

NADP⁺ Content of Bacterial FNRiloopΔW248. Unexpectedly, NADP⁺ was found bound in the crystal structure of the bacterial FNR variant. The NADP⁺ molecule is observed interacting with the protein according to an overall conserved pattern as found in other bacterial FNRs. ^{28,32} The HPLC analysis of the wild-type and mutant bacterial FNRs showed that all contain \sim 0.1 mol of nucleotide/mol of enzyme. This observation is in agreement with the similar $K_{\rm d}$ for the FNR-NADP $^+$ complexes measured for the different enzyme forms. If indeed there is no significant difference in NADP $^+$ association constant between bacterial and plastidic FNRs, crystallization might be acting as a purification step, ultimately allowing only for NADP $^+$ -bound bacterial FNRiloop Δ W248 molecules to crystallize under the particular crystallization condition that we have used.

Effects of the Deletion of the Carboxyl-Terminal Tryptophan and Insertion of the β -Hairpin on the Activity of Bacterial FNR with Its Natural Substrates. An unexpected result was the decrease in the catalytic activity of the bacterial FNR variants with the natural protein electron carriers. This effect appeared when the tryptophan was deleted and was not the result of changes of the affinity of the protein substrate (Table S2 of the Supporting Information). Consequently, it can be concluded that for the bacterial FNR the carboxyl-terminal tryptophan itself is important for efficient electron transfer with an Fd or Fld electron acceptor. A possible explanation is that the mutation modifies the proper orientation of partner protein binding and hence the electron transfer process. Another possible explanation is that the loss in the mutants of the intramolecular hydrogen bond between N1 of the isoalloxazine ring and N6 of adenine, 5,6 when the FAD acquires an open structure, is important for catalysis. The electrostatic repulsion resulting from the negative charge at N1 of the reduced flavin ring and some neighboring residues has been implicated as the source of instability of the fully reduced plastidic reductases.³⁵ When the isoalloxazine is reduced to a semiquinone form, N1 is negatively

charged, and a hydrogen bond in that atom should influence flavin reactivity. It is thus possible to propose that the transfer of electrons from NADPH to the acceptor protein Fd or Fld includes a first stage in which the FAD should be mobilized, disrupting the intramolecular hydrogen bond. Then, the interaction between N6 of the adenine ring and N1 is re-established. The latter interaction may be necessary for the reaction to occur in an efficient way and probably favors the directionality that was previously described. ²⁵

Conclusions. This work illustrates some of the structural and functional roles of the β -hairpin between amino acids 112 and 124 from plastidic FNRs and the carboxy-terminal tryptophan of the bacterial FNRs. The β -hairpin undoubtedly plays a structural role by increasing the affinity of the enzyme for FAD. The presence of an aromatic amino acid interacting with the adenine of FAD is required to stabilize the prosthetic group in plastidic and bacterial enzymes. However, the folding status of the FAD would be determined not only by the presence of the latter aromatic amino acid but also by other structural elements of each enzyme. Moreover, the overall structures of the plastidic and bacterial enzymes are not affected by changes in the β -hairpin region, provided the FAD is bound.

The high catalytic efficiency of plastidic FNR was more influenced by the loss of the $112-123~\beta$ -hairpin rather than by the inclusion of a C-terminal tryptophan. Nevertheless, other structural factors may also contribute to the realization of highly efficient enzymes. In the bacterial FNR, the catalytic behavior was not affected by the engineered introduction of the $112-123~\beta$ -hairpin. The presence of a terminal tryptophan appears to be the main determinant of low catalytic efficiency in these enzymes. In addition, this terminal amino acid seems to be relevant for the catalytic processes involving physiological protein substrates. Thus, although bacterial and plastidic FNRs display highly conserved overall architecture, subtle structural changes that influence the access of the NADP(H) to the catalytic site have a great impact on the catalytic behavior of these enzymes.

ASSOCIATED CONTENT

Supporting Information. Construction of the different plastidic and bacterial FNR variants and the sequences of the oligonucleotides used for cloning and mutagenesis (text and Table S1, respectively), dissociation constants of wild-type and mutants bacterial FNRs for ferredoxins and flavodoxin (Table S2), Fourier electron density map for the FAD molecule and key interacting residues in FNR chain A (Figure S1), Fourier electron density map for the FAD molecule (chain A) and a symmetry-related neighbor, including also detailed information on *B* factors (Figure S2). This material is available free of charge via the Internet at http://pubs.acs.org.

Accession Codes

The atomic coordinates and structure factors have been deposited in the Protein Data Bank as entries 2XNC and 2XNJ.

■ AUTHOR INFORMATION

Corresponding Author

*IBR, CONICET, Facultad de Ciencias Bioquímicas y Farmacéuticas, UNR, Suipacha 531. S2002LRK Rosario, Argentina. Fax: +54 341 4390465. Tel: +54 341-4351235. E-mail: ceccarelli@ibr.gov.ar.

Funding Sources

This work was supported by grants from CONICET and the Agencia de Promoción Científica y Tecnológica (ANPCyT), Argentina. E.A.C. is a staff member of the Consejo Nacional de Investigaciones Científicas y Técnicas (CONICET, Argentina). M.A.M. is a fellow of the same institution. Financial and logistic support from the Institut Pasteur de Montevideo (Protein Crystallography Facility PXF), the Amsud/Pasteur network, and the Center of Structural Biology of the Mercosur (CeBEM) is gratefully acknowledged.

■ ACKNOWLEDGMENT

We thank Dr. Yasuhiro Takahashi for the generous gift of the *E. coli* iron—sulfur gene cluster and Dr. Mario Ermácora for the helpful discussions about protein folding.

ABBREVIATIONS

FNR, ferredoxin-NADP(H) reductase; Fd, ferredoxin from pea; Fdx, ferredoxin from *E. coli*; Fld, flavodoxin A from *E. coli*; PDB, Protein Data Bank; rmsd, root-mean-square deviation.

REFERENCES

- (1) Ceccarelli, E. A., Arakaki, A. K., Cortez, N., and Carrillo, N. (2004) Functional plasticity and catalytic efficiency in plant and bacterial ferredoxin-NADP(H) reductases. *Biochim. Biophys. Acta* 1698, 155–165.
- (2) Carrillo, N., and Ceccarelli, E. A. (2003) Open questions in ferredoxin-NADP⁺ reductase catalytic mechanism. *Eur. J. Biochem.* 270, 1900–1915 (and references cited therein).
- (3) Aliverti, A., Pandini, V., Pennati, A., de, R. M., and Zanetti, G. (2008) Structural and functional diversity of ferredoxin-NADP⁺ reductases. *Arch. Biochem. Biophys.* 474, 283–291.
- (4) Karplus, P. A., and Faber, H. R. (2004) Structural Aspects of Plant Ferredoxin:NADP⁺ Oxidoreductases. *Photosynth. Res.* 81, 303–315.
- (5) Ingelman, M., Bianchi, V., and Eklund, H. (1997) The three-dimensional structure of flavodoxin reductase from *Escherichia coli* at 1.7 Å resolution. *J. Mol. Biol.* 268, 147–157.
- (6) Nogues, I., Perez-Dorado, I., Frago, S., Bittel, C., Mayhew, S. G., Gomez-Moreno, C., Hermoso, J. A., Medina, M., Cortez, N., and Carrillo, N. (2005) The ferredoxin-NADP(H) reductase from *Rhodobacter capsulatus*: Molecular structure and catalytic mechanism. *Biochemistry* 44, 11730–11740.
- (7) Wan, J. T., and Jarrett, J. T. (2002) Electron acceptor specificity of ferredoxin (flavodoxin):NADP⁺ oxidoreductase from *Escherichia coli*. *Arch. Biochem. Biophys.* 406, 116–126.
- (8) Catalano Dupuy, D. L., Rial, D. V., and Ceccarelli, E. A. (2004) Inhibition of pea ferredoxin-NADP(H) reductase by Zn-ferrocyanide. *Eur. J. Biochem.* 271, 4582–4593.
- (9) Musumeci, M. A., Arakaki, A. K., Rial, D. V., Catalano-Dupuy, D. L., and Ceccarelli, E. A. (2008) Modulation of the enzymatic efficiency of ferredoxin-NADP(H) reductase by the amino acid volume around the catalytic site. *FEBS J.* 275, 1350–1366.
- (10) Nakamura, M., Saeki, K., and Takahashi, Y. (1999) Hyperproduction of recombinant ferredoxins in *Escherichia coli* by coexpression of the ORF1-ORF2-iscS-iscU-iscA-hscB-hs cA-fdx-ORF3 gene cluster. *J. Biochem.* 126, 10–18.
- (11) Hurley, J. K., Weber-Main, A. M., Hodges, A. E., Stankovich, M. T., Benning, M. M., Holden, H. M., Cheng, H., Xia, B., Markley, J. L., Genzor, C., Gomez-Moreno, C., Hafezi, R., and Tollin, G. (1997) Iron-sulfur cluster cysteine-to-serine mutants of *Anabaena* [2Fe-2S] ferredoxin exhibit unexpected redox properties and are competent in electron transfer to ferredoxin:NADP⁺ reductase. *Biochemistry* 36, 15109–15117.
- (12) Laemmli, U. K. (1970) Cleavage of structural proteins during the assembly of the head of bacteriophage T4. *Nature* 227, 680-685.

- (13) Aliverti, A., Bruns, C. M., Pandini, V. E., Karplus, P. A., Vanoni, M. A., Curti, B., and Zanetti, G. (1995) Involvement of serine 96 in the catalytic mechanism of ferredoxin-NADP⁺ reductase: Structure—function relationship as studied by site-directed mutagenesis and X-ray crystallography. *Biochemistry* 34, 8371–8379.
- (14) Catalano-Dupuy, D. L., Orecchia, M., Rial, D. V., and Ceccarelli, E. A. (2006) Reduction of the pea ferredoxin-NADP(H) reductase catalytic efficiency by the structuring of a carboxyl-terminal artificial metal binding site. *Biochemistry* 45, 13899–13909.
- (15) Santos, J., Risso, V. A., Sica, M. P., and Ermacora, M. R. (2007) Effects of serine-to-cysteine mutations on β -lactamase folding. *Biophys. J.* 93, 1707–1718.
- (16) Zanetti, G. (1976) A lysyl residue at the NADP⁺ binding site of ferredoxin-NADP⁺ reductase. *Biochim. Biophys. Acta* 445, 14–24.
- (17) Zanetti, G., Cidaria, D., and Curti, B. (1982) Preparation of apoprotein from spinach ferredoxin-NADP⁺ reductase. Studies on the resolution process and characterization of the FAD reconstituted holoenzyme. *Eur. J. Biochem.* 126, 453–458.
- (18) Navaza, J. (2001) Implementation of molecular replacement in AMoRe. *Acta Crystallogr.* D57, 1367–1372.
- (19) Murshudov, G. N., Vagin, A. A., and Dodson, E. J. (1997) Refinement of macromolecular structures by the maximum-likelihood method. *Acta Crystallogr.* D53, 240–255.
- (20) Roversi, P., Blanc, E., Vonrhein, C., Evans, G., and Bricogne, G. (2000) Modelling prior distributions of atoms for macromolecular refinement and completion. *Acta Crystallogr. D56*, 1316–1323.
- (21) Piubelli, L., Aliverti, A., Arakaki, A. K., Carrillo, N., Ceccarelli, E. A., Karplus, P. A., and Zanetti, G. (2000) Competition between C-terminal tyrosine and nicotinamide modulates pyridine nucleotide affinity and specificity in plant ferredoxin-NADP⁺ reductase. *J. Biol. Chem.* 275, 10472–10476.
- (22) Aliverti, A., Piubelli, L., Zanetti, G., Lubberstedt, T., Herrmann, R. G., and Curti, B. (1993) The role of cysteine residues of spinach ferredoxin-NADP $^+$ reductase as assessed by site-directed mutagenesis. *Biochemistry* 32, 6374–6380.
- (23) Paladini, D. H., Musumeci, M. A., Carrillo, N., and Ceccarelli, E. A. (2009) Induced fit and equilibrium dynamics for high catalytic efficiency in ferredoxin-NADP(H) reductases. *Biochemistry* 48, 5760–5768.
- (24) Tejero, J., Perez-Dorado, I., Maya, C., Martinez-Julvez, M., Sanz-Aparicio, J., Gomez-Moreno, C., Hermoso, J. A., and Medina, M. (2005) C-Terminal tyrosine of ferredoxin-NADP $^+$ reductase in hydride transfer processes with NAD(P) $^+$ /H. *Biochemistry 44*, 13477–13490.
- (25) McIver, L., Leadbeater, C., Campopiano, D. J., Baxter, R. L., Daff, S. N., Chapman, S. K., and Munro, A. W. (1998) Characterisation of flavodoxin NADP⁺ oxidoreductase and flavodoxin; key components of electron transfer in *Escherichia coli. Eur. J. Biochem.* 257, 577–585.
- (26) Deng, Z., Aliverti, A., Zanetti, G., Arakaki, A. K., Ottado, J., Orellano, E. G., Calcaterra, N. B., Ceccarelli, E. A., Carrillo, N., and Karplus, P. A. (1999) A productive NADP⁺ binding mode of ferredoxin-NADP⁺ reductase revealed by protein engineering and crystallographic studies. *Nat. Struct. Biol.* 6, 847–853.
- (27) Nascimento, A. S., Catalano-Dupuy, D. L., Bernardes, A., de Oliveira, N. M., Santos, M. A., Ceccarelli, E. A., and Polikarpov, I. (2007) Crystal structures of *Leptospira interrogans* FAD-containing ferredoxin-NADP⁺ reductase and its complex with NADP⁺. *BMC Struct. Biol.* 7, 69.
- (28) Bortolotti, A., Perez-Dorado, I., Goni, G., Medina, M., Hermoso, J. A., Carrillo, N., and Cortez, N. (2009) Coenzyme binding and hydride transfer in *Rhodobacter capsulatus* ferredoxin/flavodoxin NADP-(H) oxidoreductase. *Biochim. Biophys. Acta* 1794, 199–210.
- (29) Milani, M., Balconi, E., Aliverti, A., Mastrangelo, E., Seeber, F., Bolognesi, M., and Zanetti, G. (2007) Ferredoxin-NADP⁺ reductase from *Plasmodium falciparum* undergoes NADP⁺-dependent dimerization and inactivation: Functional and crystallographic analysis. *J. Mol. Biol.* 367, 501–513.
- (30) Tejero, J., Martinez-Julvez, M., Mayoral, T., Luquita, A., Sanz-Aparicio, J., Hermoso, J. A., Hurley, J. K., Tollin, G., Gomez-Moreno, C., and Medina, M. (2003) Involvement of the pyrophosphate and the

2'-phosphate binding regions of ferredoxin-NADP⁺ reductase in coenzyme specificity. *J. Biol. Chem.* 278, 49203–49214.

- (31) Hermoso, J. A., Mayoral, T., Faro, M., Gomez-Moreno, C., Sanz-Aparicio, J., and Medina, M. (2002) Mechanism of coenzyme recognition and binding revealed by crystal structure analysis of ferredoxin-NADP⁺ reductase complexed with NADP. *J. Mol. Biol.* 319 1133–1142.
- (32) Wang, A., Rodriguez, J. C., Han, H., Schonbrunn, E., and Rivera, M. (2008) X-ray crystallographic and solution state nuclear magnetic resonance spectroscopic investigations of NADP⁺ binding to ferredoxin-NADP⁺ reductase from *Pseudomonas aeruginosa*. *Biochemistry* 47, 8080–8093.
- (33) Leadbeater, C., McIver, L., Campopiano, D. J., Webster, S. P., Baxter, R. L., Kelly, S. M., Price, N. C., Lysek, D. A., Noble, M. A., Chapman, S. K., and Munro, A. W. (2000) Probing the NADPH-binding site of *Escherichia coli* flavodoxin oxidoreductase. *Biochem. J.* 352 (Part 2), 257–266.
- (34) Nogues, I., Tejero, J., Hurley, J. K., Paladini, D., Frago, S., Tollin, G., Mayhew, S. G., Gomez-Moreno, C., Ceccarelli, E. A., Carrillo, N., and Medina, M. (2004) Role of the C-terminal tyrosine of ferredoxin-nicotinamide adenine dinucleotide phosphate reductase in the electron transfer processes with its protein partners ferredoxin and flavodoxin. *Biochemistry* 43, 6127–6137.
- (35) Martinez-Julvez, M., Tejero, J., Peregrina, J. R., Nogues, I., Frago, S., Gomez-Moreno, C., and Medina, M. (2005) Towards a new interaction enzyme:coenzyme. *Biophys. Chem.* 115, 219–224.